Science and Technology of Advanced Materials

ISSN: 1468-6996 (Print) 1878-5514 (Online) Journal homepage: www.tandfonline.com/journals/tsta20

Sum rules for X-ray circular and linear dichroism based on complete magnetic multipole basis

Y. Yamasaki, Y. Ishii & N. Sasabe

To cite this article: Y. Yamasaki, Y. Ishii & N. Sasabe (2025) Sum rules for X-ray circular and linear dichroism based on complete magnetic multipole basis, Science and Technology of Advanced Materials, 26:1, 2513217, DOI: 10.1080/14686996.2025.2513217

To link to this article: https://doi.org/10.1080/14686996.2025.2513217

Published online: 30 Jun 2025.

SCIENCE AND TECHNOLOGY OF ADVANCED MATERIALS
2025, VOL. 26, NO. 1, 2513217
https://doi.org/10.1080/14686996.2025.2513217

Taylor & Francis
Taylor & Francis Group

Sum rules for X-ray circular and linear dichroism based on complete magnetic multipole basis

Y. Yamasaki [a,b,c], Y. Ishii[a] and N. Sasabe[a]

[a]Center for Basic Research on Materials, National Institute for Materials Science (NIMS), Tsukuba, Japan;
[b]International Center for Synchrotron Radiation Innovation Smart, Tohoku University, Sendai, Japan;
[c]Center for Emergent Matter Science (CEMS), RIKEN, Wako, Japan

ABSTRACT

X-ray magnetic circular dichroism (XMCD) and X-ray magnetic linear dichroism (XMLD) are powerful spectroscopic techniques for probing magnetic properties in solids. In this study, we revisit the XMCD and XMLD sum rules within a complete magnetic multipole basis that incorporates both spinless and spinful multipoles. We demonstrate that these multipoles can be clearly distinguished and individually detected through the sum-rule formalism. Within this framework, the anisotropic magnetic dipole term is naturally derived in XMCD, offering a microscopic origin for ferromagnetic-like behavior in antiferromagnets. Furthermore, we derive the sum rules for out-of-plane and in-plane XMLD regarding electric quadrupole contributions defined based on the complete multipole basis. Our theoretical approach provides a unified, symmetry-consistent framework for analyzing dichroic signals in various magnetic materials. These findings deepen the understanding of XMCD and XMLD and open pathways to exploring complex magnetic structures and spin-orbit coupling effects in emergent magnetic materials.

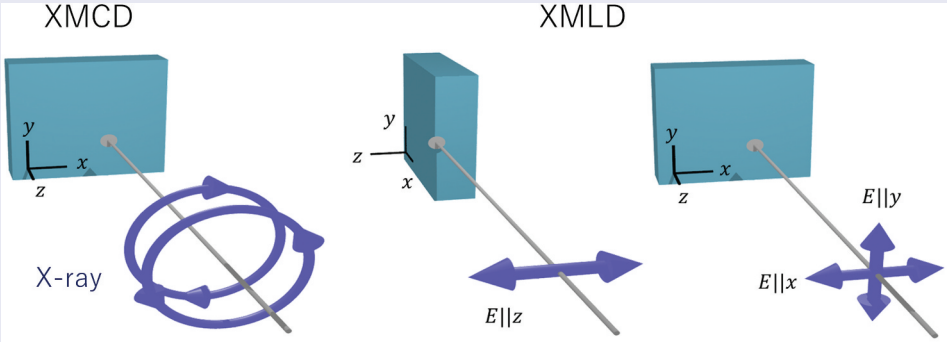

XAS/XMCD/XMLD sum rules based on the complete multipole basis

$$S_{lm}^{j\pm} = \alpha_{\pm}^{(0)}\beta_{l}^{(0,l)}\langle \underline{X}_{lm}^{(0,0)}\rangle + \alpha_{\pm}^{(1)}\beta_{l}^{(1,l-1)}\langle \underline{X}_{lm}^{(1,-1)}\rangle - \alpha_{\pm}^{(1)}\beta_{l}^{(1,l+1)}\langle \underline{X}_{lm}^{(1,1)}\rangle$$

IMPACT STATEMENT

Unified XMCD/XMLD/XAS sum rules on a complete magnetic multipole basis, disentangling spinless and spinful channels, providing a powerful tool to uncover the microscopic origins of altermagnets and other emergent magnetic states.

ARTICLE HISTORY
Received 23 April 2025
Revised 19 May 2025
Accepted 26 May 2025

KEYWORDS
Magnetic materials; X-ray absorption spectroscopy; X-ray magnetic circular dichroism; X-ray magnetic linear dichroism; Altermagnet

1. Introduction

1.1. X-ray absorption spectroscopy

X-ray absorption spectroscopy (XAS) is a powerful tool for investigating the electronic and magnetic properties of materials [1]. Among its various techniques, X-ray Magnetic Circular Dichroism (XMCD) and X-ray Magnetic Linear Dichroism (XMLD) have been extensively applied in synchrotron-based experiments to investigate element-specific information on magnetism [2–5]. XMCD is a phenomenon where the absorption of circularly polarized X-rays differs depending on the relative orientation of the photon helicity and the magnetization. This effect arises from the spin-orbit interaction in the core-level states, leading to different transition probabilities for left- and

CONTACT Y. Yamasaki Yamasaki.Yuichi@Nims.Go.Jp Center for Basic Research on Materials, National Institute for Materials Science (NIMS), Tsukuba 305-0047, Japan

right-circularly polarized light. XMCD is widely used to determine element-specific spin and orbital magnetic moments via sum rules [6–9].

It has been extensively applied to transition metal and rare-earth compounds to study magnetic ordering, local electronic structure, and hybridization effects. XMCD has played a crucial role in understanding magnetic thin films, multilayers, and nanostructures, especially in spintronics and permanent magnets [5,10–13]. Due to its sensitivity to both spin and orbital contributions to magnetism, XMCD enables separating these components [14], which is essential for studying phenomena such as spin-orbit coupling and anisotropy in magnetic materials.

In contrast to XMCD, XMLD refers to the difference in X-ray absorption between two orthogonal linear polarizations in a magnetically ordered system [15,16]. XMLD is primarily sensitive to the anisotropy of the local electronic structure and provides information about orbital occupation and magnetic ordering. Unlike XMCD, which directly probes net magnetization, XMLD is particularly useful for investigating antiferromagnetic and non-collinear magnetic structures. XMLD arises from the anisotropic valence state due to the spin-orbit and exchange interactions, leading to an anisotropic absorption cross-section. This makes XMLD a valuable tool for studying magnetocrystalline anisotropy, spin reorientation transitions, and antiferromagnetic domain structures in materials such as transition metal oxides and rare-earth compounds.

1.2. Magnetic dipole order in antiferromagnet

Recent studies in magnetism have revealed that phenomena traditionally associated with ferromagnets, such as the anomalous Hall effect (AHE), the magneto-optical Kerr effect (MOKE), and XMCD can emerge even in antiferromagnetic materials, provided that the magnetic ordering symmetry allows for magnetic dipole components. This behavior has been observed in both non-collinear antiferromagnets, such as Mn_3Sn [17,18], and collinear antiferromagnets recently classified as altermagnets, including manganese oxides [19–21], organic antiferromagnetic [22], RuO_2 [23–26] and MnTe [27,28]. In these systems, although the net magnetization vanishes in real space, the presence of symmetry-allowed magnetic dipole moments, *i.e.* specifically the anisotropic magnetic dipole term (t_z), enables ferromagnetic-like responses such as AHE and XMCD to appear [29–33]. This underscores that the key condition for the emergence of these effects is not the specific spin configuration (collinear or non-collinear), but the magnetic dipole symmetry permitted by the crystal and magnetic structure. These observations collectively emphasize that optical responses such as XMCD do not directly probe the net magnetization, but are determined by the magnetic multipole symmetry inherent to the system. Therefore, to properly interpret the spectroscopic signals, including XAS and XMLD, it is essential to establish the corresponding sum rules within a complete magnetic multipole framework, ensuring all contributions from hidden multipole moments.

1.3. Complete multipole basis

Multipole expansions systematically describe various physical properties, such as charge and magnetic distributions, in condensed matter systems. The conventional classification distinguishes between electric multipoles $\boldsymbol{Q}$ (arising from charge distributions) and magnetic multipoles $\boldsymbol{M}$ (associated with current and spin distributions). However, recent developments by Hayami and Kusunose et al., have established a complete magnetic multipole basis that extends this classification to include electric toroidal multipoles $\boldsymbol{G}$ and magnetic toroidal multipoles $\boldsymbol{T}$ [34,35]. The multipole representation of four-type multipoles enables a comprehensive understanding of various electronic properties and physical phenomena observed in materials.

The general form of a multipole operator in spinless Hilberlt space is expressed as $\hat{X}^{(\mathrm{orb})}_{lm}$ where l and m denote the quantum numbers of the orbital angular momentum, and X represents the type of multipole ($\boldsymbol{X} = \boldsymbol{Q}, \boldsymbol{M}, \boldsymbol{T}, \boldsymbol{G}$). The multipole operator in the spinful space is obtained by angular momentum coupling between the spinless multipole and the spin angular momentum [34,35], which is given by

$$\hat{X}^{(s,k)}_{lm} \equiv i^{s+k} \sum_{n=-s}^{s} C^{lm}_{l+k,m-n;sn} \hat{X}^{(\mathrm{orb})}_{l+k,m-n} \hat{\sigma}_{sn} \qquad (1)$$

where $C^{lm}_{l_1,m_1;l_2,m_2}$ is the Clebsh-Gordan coefficient, $s = 0, 1$ and $-s \leq k \leq s$ (k is integer). The spin operator is expressed using the Pauli matrices σ_{sn} in the spin space, defined as $\sigma_{00} = \sigma_0$ (the identity matrix), $\sigma_{10} = \sigma_z$, and $\sigma_{1,\pm1} = \mp(\sigma_x \pm i\sigma_y)/\sqrt{2}$. Magnetic multipoles are classified based on their transformation properties under spatial inversion ($\mathcal{I}$) and time-reversal ($\mathcal{T}$) symmetry. In this paper, we focus only on multipoles that possess spatial inversion symmetry ($\mathcal{I}$), namely, electric monopoles Q_{00}, magnetic dipoles M_{1m}, and electric quadrupoles Q_{2m}.

Spinless multipoles ($s = 0$) are expressed as $\hat{X}^{(0,0)}_{lm} \equiv \hat{X}^{(\mathrm{orb})}_{lm} \sigma_0$. Since σ_0 is the identity matrix, the type of magnetic multipole basis coincides with that of the orbital multipole basis, namely, $\hat{Q}^{(0,0)}_{lm} = \hat{Q}^{(\mathrm{orb})}_{lm}$ and $\hat{M}^{(0,0)}_{lm} = \hat{M}^{(\mathrm{orb})}_{lm}$. On the other hand, in the spinful space ($s = 1$), since the time-reversal symmetry of spin is odd, the time-reversal symmetry of $\hat{X}^{(1,k)}_{lm}$ should be opposite to that of $\hat{X}^{(\mathrm{orb})}_{lm}$. In addition, since the spin is

the axial vector, a spinful multipole is composed of orbital multipoles with different spatial parity. For example, the electric multipole ($\hat{X}=\hat{Q}$) contains three spinful multipoles ($s=1$, $k=-1,0,1$),

$$\hat{Q}_{lm}^{(1,0)} = i\sum_{n} C_{l,m-n;1n}^{lm}\hat{T}_{l,m-n}^{(orb)}\hat{\sigma}_{1n}, \tag{2}$$

$$\hat{Q}_{lm}^{(1,\pm1)} = i^{1\pm1}\sum_{n} C_{l\pm1,m-n;1n}^{lm}\hat{M}_{l\pm1,m-n}^{(orb)}\hat{\sigma}_{1n}, \tag{3}$$

suggesting that spinful charge multipoles are generated from the combination of magnetic toroidal moments with the same l ($\hat{T}_l$) and magnetic multipoles with l differing by one ($\hat{M}_{l\pm1}$). As well as, the magnetic multipole ($\hat{X}=\hat{M}$) has

$$\hat{M}_{lm}^{(1,0)} = i\sum_{n} C_{l,m-n;1n}^{lm}\hat{G}_{l,m-n}^{(orb)}\sigma_{1n}, \tag{4}$$

$$\hat{M}_{lm}^{(1,\pm1)} = i^{1\pm1}\sum_{n} C_{l\pm1,m-n;1n}^{lm}\hat{Q}_{l\pm1,m-n}^{(orb)}\sigma_{1n}, \tag{5}$$

indicating that spinful charge multipoles are generated from the combination of electronic toroidal moments with the same l ($\hat{G}_l$) and electric charge multipoles with l differing by one ($\hat{Q}_{l\pm1}$). The relationship between these complete magnetic multipole bases and the spinless and spinful bases is summarized in Table 1.

The matrix element of $\hat{X}_{lm}^{(s,k)}$ on $|l_v, m_v; \frac{1}{2}m_s\rangle$ basis is given by

$$\begin{aligned}&\langle l_v m_v^{'};\frac{1}{2}m_s^{'}|\hat{X}_{lm}^{(s,k)}|l_v m_v;\frac{1}{2}m_s\rangle \\ &= i^{s+k}C_{\kappa\mu;sn}^{lm}C_{l_v m_v;\kappa\mu}^{l_v m_v^{'}}C_{\frac{1}{2}m_s;sn}^{\frac{1}{2}m_s^{'}}\frac{\langle l_v||\hat{X}_{\kappa}^{(\mathrm{orb})}||l_v\rangle}{\sqrt{2l_v+1}}\end{aligned} \tag{6}$$

with $\kappa \equiv l+k$ and $\mu-n$. $\langle l_v||\hat{X}_{\kappa}^{(\mathrm{orb})}||l_v\rangle$ is the reduced matrix element, whose explicit expression for $X=Q$ and M are given in Equation 8 and Equation 9 in Ref [34]. Using the spherical tensor for multipole for $l=0,1,2,\cdots$ and its z-component $m=-l,-l+1,\cdots,l$,

$$O_{lm} \equiv \sqrt{\frac{4\pi}{2l+1}}r^l Y_{lm}(\hat{r}) \tag{7}$$

with $\hat{r}=\boldsymbol{r}/r$ and the spherical harmonics Y_{lm}, the electronic and magnetic multipoles are given by $Q_{lm}^{(\mathrm{orb})}=O_{lm}$ and

$$M_{l,m}^{(\mathrm{orb})} = \frac{1}{2}\left[(\nabla O_{lm})\cdot\hat{m}_l + \hat{m}_l\cdot(\nabla O_{lm})\right] \tag{8}$$

with $\hat{m}_l = 2\hat{\boldsymbol{l}}/(l+1)$, respectively. For example, O_{lm} corresponding to the magnetic dipole ($l=1$) and octupole ($l=3$) can be explicitly given in Table 2.

2. Theoretical framework of X-ray absorption

In recent decades, the development of sum rules for X-ray absorption spectroscopy has significantly advanced our understanding of the electronic and magnetic properties. Sum rules link the integrated intensity of XAS and dichroism spectra to ground-state quantities such as spin, orbital magnetic moments, and charge distribution. These relationships have provided profound insights into magnetic anisotropy, spin-orbit coupling, and electronic correlations. This work presents sum rules for X-ray absorption based on the complete magnetic multipole bases.

The theoretical framework for X-ray absorption for electric dipole transition is rooted in the Fermi Golden Rule, which relates the absorption coefficient to the transition probability $\mu_{\varepsilon}(\hbar\omega)$ defined by

Table 1. Classification of spinful multiples ($s=1$) with the inversion symmetry, *i.e.* electric monopole, magnetic dipole, and electric quadrupole moment, for possible k parameters.

(s,k)	$(1,-1)$	$(1,0)$	$(1,1)$
$Q_{00}^{(s,k)}$	-	-	$-C_{1,m-n;1n}^{00}M_{1,m-n}^{(\mathrm{orb})}\sigma_{1n}$
$M_{1m}^{(s,k)}$	$C_{0,m-n;1n}^{1m}Q_{0,m-n}^{(\mathrm{orb})}\sigma_{1n}$	$iC_{1,m-n;1n}^{1m}G_{1,m-n}^{(\mathrm{orb})}\sigma_{1n}$	$-C_{2,m-n;1n}^{1m}Q_{2,m-n}^{(\mathrm{orb})}\sigma_{1n}$
$Q_{2m}^{(s,k)}$	$C_{1,m-n;1n}^{2m}M_{1,m-n}^{(\mathrm{orb})}\sigma_{1n}$	$iC_{2,m-n;1n}^{2m}T_{2,m-n}^{(\mathrm{orb})}\sigma_{1n}$	$-C_{3,m-n;1n}^{2m}M_{3,m-n}^{(\mathrm{orb})}\sigma_{1n}$

Table 2. Explicit expression of O_{lm} relating magnetic dipole ($l=1$) and octupole ($l=3$) with the position operator $\boldsymbol{r}=(x,y,z)$ and the unit vector $\boldsymbol{e}=(e_x,e_y,e_z)$.

(l,m)	O_{lm}
$(1,\pm1)$	$\mp\frac{1}{2}(e_x \pm ie_y)$
$(1,0)$	e_z
$(3,\pm3)$	$\mp\frac{3\sqrt{5}}{4}(x\pm iy)^2(e_x\pm ie_y)$
$(3,\pm2)$	$\frac{1}{2}\sqrt{\frac{15}{2}}(x\pm iy)\left[2z(e_x\pm ie_y)+(x\pm iy)e_z\right]$
$(3,\pm1)$	$\mp\frac{\sqrt{3}}{4}\left[(5z^2-r^2)(e_x\pm ie_y)+2(x\pm iy)(5ze_z-r)\right]$
$(3,0)$	$-3z(xe_x+ye_y)+\frac{3}{2}(3z^2-r^2)e_z$

Table 3. Classification of sum rules for X-ray absorption spectrum (XAS), X-ray magnetic circular dichroism (XMCD), and X-ray magnetic linear dichroism (XMLD) based on the complete multipole basis.

Technique	l	m	s	k	multipole basis	sum rule
XAS	0	0	0	0	$Q^{(orb)}_{00}\sigma_0$	n_h
			1	1	$M^{(orb)}_{1,-n}\sigma_{1n}$	$\underline{\hat{\boldsymbol{l}}}\cdot\underline{\hat{\boldsymbol{s}}}$
XMCD	1	m	0	0	$M^{(orb)}_{1,m}\sigma_0$	$\underline{l}_z$
			1	−1	$Q^{(orb)}_{0,0}\sigma_{1n}$	$\underline{s}_z$
			1	1	$Q^{(orb)}_{2,m-n}\sigma_{1n}$	$[\underline{\boldsymbol{Q}}\otimes\underline{\boldsymbol{s}}]_z$
XMLD	2	m	0	0	$Q^{(orb)}_{2,m}\sigma_0$	$\underline{Q}_{3z^2-r^2}, \underline{Q}_{x^2-y^2}$
			1	−1	$M^{(orb)}_{1,m-n}\sigma_{1n}$	$[\underline{\boldsymbol{l}}\otimes\underline{\boldsymbol{s}}]_z$
			1	1	$M^{(orb)}_{3,m-n}\sigma_{1n}$	$[\underline{\boldsymbol{M}}^{(orb)}_3\otimes\underline{\boldsymbol{s}}]_z$

$$\mu_\varepsilon(\hbar\omega)\equiv\sum_{f,M}\left|\langle\psi_f|\boldsymbol{E}\cdot\boldsymbol{r}|\psi_g\rangle\right|^2\delta(E_f-E_g-\hbar\omega), \quad (9)$$

with polarization vector $\boldsymbol{E}=E_0\varepsilon$ of the incident x-ray polarization and position operator $\boldsymbol{r}$. They can be expanded as the vector product in terms of spherical tensor operators,

$$\boldsymbol{E}\cdot\boldsymbol{r}=E_0\sum_{M=-1}^{1}(-1)^M\varepsilon_{-M}r_M \quad (10)$$

where r_M is the spherical tensors of rank 1, and $\varepsilon_{\pm1}=\mp(\varepsilon_x\pm i\varepsilon_y)/\sqrt{2}$ and $\varepsilon_0=\varepsilon_z$, corresponding to the circular and linear polarization, respectively. E_g (E_f) indicates the energy of initial (final) states, and $\hbar\omega$ is the photon energy. $|\psi_g\rangle=|\psi(l_v^n)\rangle$ denotes any state of the ground configuration of the outer shell, *i.e.* a valence electronic state of n electrons with the azimuthal angular momentum l_v. The final state configuration is represented by $|\psi_f\rangle=|\underline{c}_{jm}\psi'(l_v^{n+1})\rangle$ where $\underline{c}_{jm}$ stands for a hole in a core level. This formulation captures the core-level transitions induced by the electric multipole interaction, which dominates in XAS experiments.

The integral of XAS concerning the electric dipole transition from a core state with $j_\pm=l_c\pm\frac{1}{2}$ is expressed as

$$I^{j\pm}_\varepsilon=\int_{j_\pm}\mu_\varepsilon(\hbar\omega)d\omega=\sum_{MM'}E_0^2(-1)^{M+M'}\varepsilon^*_{-M'}\varepsilon_{-M}P^{j\pm}_{M'M} \quad (11)$$

with

$$P^{j\pm}_{M'M}\equiv\sum_{f\in j_\pm}\langle\psi_g|r^*_{M'}|\psi_f\rangle\langle\psi_f|r_M|\psi_g\rangle. \quad (12)$$

Using the Wigner-Eckart theorem, the matrix element of photoelectron transition from the core state jm_j to the valence state l_vm_v by the electric dipole moment r_M is given by

$$\langle\psi_f|r_M|\psi_g\rangle=\sum_{\{m\}}C^{l_vm_v}_{l_cm_c;1M}C^{jm_j}_{l_cm_c;\frac{1}{2}m_s}\frac{\langle\psi_f|a^\dagger_{m_vm_s}b_{jm_j}|\psi_g\rangle}{\sqrt{2l_v+1}}\langle l_v||O_1||l_c\rangle_R \quad (13)$$

where $C^{l_3m_3}_{l_1m_1;l_2m_2}$ is the Clebsh-Gordan coefficient and the index of $\{m\}$ indicates the summation for all m.

Here, b_{jm_j} ($b^\dagger_{jm_j}$) denotes the annihilation (creation) operator acting on core-electron states characterized by quantum numbers j, m_j, whereas $a_{m_vm_s}$ ($a^\dagger_{m_vm_s}$) refers to the annihilation (creation) operator for valence states labeled by m_v, m_s. In addition, $\langle l_v||O_1||l_c\rangle_R$ denotes the reduced matrix element, which in this paper is approximated as independent of m and energy. The Wigner – Eckart theorem establishes the selection rules for electric dipole transitions: $l_c-l_v=0,\pm1$, $m_c-m_v=0,\pm1$, and the spin of both the core and valence states is conserved.

By substituting Equation 12 into Equation 11, $P^{j\pm}_{M'M}$ can be rewritten as

$$P^{j\pm}_{M'M}=\sum_{\psi_f}\sum_{\{m\}}[l_v]^{-1}C^{l_vm_v}_{l_cm_c;1M}C^{jm_j}_{l_cm_c;\frac{1}{2}m_s}C^{l_vm'_v}_{l_cm'_c;1M'}C^{jm'_j}_{l_cm'_c;\frac{1}{2}m'_s}\times\langle\psi_g|b^\dagger_{jm_j}a_{m_vm_s}|\psi_f\rangle\langle\psi_f|a^\dagger_{m'_vm'_s}b_{jm'_j}|\psi_g\rangle R_{l_c} \quad (14)$$

with $[l_v]\equiv2l_v+1$ and $R_{l_c}=|\langle l_v||O_1||l_c\rangle_R|^2$. By taking the sum over m_j while noting that $m'_j=m_j$ for the absorption process, we arrive at the following equation 1:

$$P^{j\pm}_{M'M}=\sum_{\{m\}}\sum_{s=0}^{1}\sum_{n=-s}^{s}\frac{\alpha^{(s)}_\pm(l_c)}{[l_cl_v]}C^{l_vm_v}_{l_cm_c;1M}C^{l_vm'_v}_{l_cm'_c;1M'}C^{l_cm_c}_{l_cm'_c;s,-n}C^{\frac{1}{2}m_s}_{\frac{1}{2}m'_s;sn}R_{l_c} \quad (15)$$

with $[ab\cdots]\equiv(2a+1)(2b+1)\cdots$. Here, $\alpha^{(s)}_\pm(l_c)$ is a coefficient depending on the core state $j_\pm=l_c\pm1/2$ and expressed as

$$\alpha_{\pm}^{(s)}(l_c) = \begin{pmatrix} j_{\pm} + \frac{1}{2} & (s=0) \\ \pm\sqrt{3l_c(l_c+1)} & (s=1). \end{pmatrix} \quad (16)$$

This parameter implies that the absorption intensity can be divided into processes in which the spin does not flip $(s=0)$ and those where the spin flips $(s=1)$. By summing the absorption intensities from both $j_{\pm}$, the spin-flip processes cancel out, leaving only the information from the spin nonflip process. By calculating the absorption intensity for $j_{\pm}$ separately and taking the appropriate difference, the information on the spin-flop process can be obtained. In other words, observing the absorption process of the spin-flop transition requires absorption in the inner core levels split by the spin-orbit interaction.

3. Polarization sum rules of X-ray absorption

To relate X-ray absorption to the physical symmetry of the holes in the valence state, here, we introduce a multipole with the quantum numbers l and m defined as

$$S_{lm}^{j\pm} \equiv \sum_{MM'} C_{1M';lm}^{1M} P_{M'M}^{j\pm}, \quad (17)$$

giving some descriptions of the sum of XAS with different X-ray polarizations. The sum of XAS for isotropic polarization is linked to the electric monopole, which is confirmed by $S_{00}^{j\pm} = I_z^{j\pm} + I_+^{j\pm} + I_-^{j\pm}$ due to $C_{1M';00}^{1M} = \delta_{MM'}$. The dipole moment quantum number gives $S_{10}^{j\pm} = \frac{1}{\sqrt{2}}(I_-^{j\pm} - I_+^{j\pm})$ due to $C_{1M';10}^{1M} = \frac{1}{\sqrt{2}} M \delta_{MM'}$, which corresponds to XMCD when the incident X-ray is aligned along the z axis. In addition, we consider (i) perpendicular and (ii) in-plane X-ray magnetic linear dichroism (XMLD). The perpendicular XMLD is expressed by a quadrupole moment $S_{20}^{j\pm} = \frac{1}{\sqrt{10}}(I_+^{j\pm} + I_-^{j\pm} - 2I_z^{j\pm})$, representing the difference in XAS with linear polarization between the perpendicular and in-plane directions. In contrast, the in-plane XMLD, i.e. the difference in XAS with linear polarization between the in-plane x- and y-directions, can not be described by a single S_{lm}. However, using a relation of $S_{2,\pm 2}^{j\pm} = \frac{3}{\sqrt{15}} P_{\pm 1,\mp 1}^{j\pm}$, it is confirmed that its difference is linked to the in-plane XMLD as $S_{2,2}^{j\pm} + S_{2,-2}^{j\pm} = \frac{3}{\sqrt{15}}(I_y^{j\pm} - I_x^{j\pm})$ as discussed below.

Substituting Equation 11 into Equation 16 results in a product of four Clebsch-Gordan coefficients involving summation over m_c, m_c', M, and M'. By applying the transformation formula for the Wigner-9j symbol2, Equation 16 can be rewritten as

$$S_{lm}^{j\pm} = \sum_{s,\kappa} \sum_{n,\mu} \sum_{\{m\}} \alpha_{\pm}^{(s)} \beta_l^{(s,\kappa)} \langle \psi_g | C_{\kappa\mu;sn}^{lm} C_{l_v m_v';\kappa\mu}^{l_v m_v} C_{\frac{1}{2}m_s';sn}^{\frac{1}{2}m_s} a_{m_v m_s} a_{m_v' m_s'}^{\dagger} | \psi_g \rangle \quad (18)$$

where $s = 0, 1$ and $|s-l| \le \kappa \le \min(2l_v, s+l)$ (κ is integer). The coefficient $\beta_l^{(s,\kappa)}$ is independent of any m and expressed using the Wigner-9j symbol as

$$\beta_l^{(s,\kappa)}(l_c, l_v, L) \equiv \frac{[\kappa][L]^{\frac{1}{2}}}{[l_c l_v l]^{\frac{1}{2}}} \begin{Bmatrix} l_v & l_c & L \\ l_v & l_c & L \\ k & s & l \end{Bmatrix} R_{l_c} \quad (19)$$

where $[ab\cdots]^{\frac{1}{2}} \equiv \{(2a+1)(2b+1)\cdots\}^{\frac{1}{2}}$ and $\{\dot{\cdots}\}$ indicate the Wigner-9j symbols. Here, we consider a complete multipole operator for holes in the valence of the ground state $|\psi_g\rangle$ expressed by $\underline{\hat{X}}_{lm}^{(s,k)}$ based on the analogy of Equation 1. Consequently, the sum of XAS at $j_{c\pm} = l_c \pm \frac{1}{2}$ core state can be rewritten by using the expectation value of complete magnetic multipoles for holes and Equation 6 as

$$S_{lm}^{j\pm} = \alpha_{\pm}^{(0)} \beta_l^{(0,l)} \langle \underline{X}_{lm}^{(0,0)} \rangle + \alpha_{\pm}^{(1)} \beta_l^{(1,l-1)} \langle \underline{X}_{lm}^{(1,-1)} \rangle - \alpha_{\pm}^{(1)} \beta_l^{(1,l+1)} \langle \underline{X}_{lm}^{(1,1)} \rangle, \quad (20)$$

with

$$\langle \underline{X}_{lm}^{(s,k)} \rangle \equiv \sum_{n,\mu} \sum_{\{m\}} i^{s+k} \langle \psi_g | C_{\kappa\mu;sn}^{lm} C_{l_v m_v';\kappa\mu}^{l_v m_v} C_{\frac{1}{2}m_s';sn}^{\frac{1}{2}m_s} a_{m_v m_s} a_{m_v' m_s'}^{\dagger} | \psi_g \rangle.$$

Since $\langle \underline{X}_{lm}^{(s,k)} \rangle$ contains only the expectation value for angular information of the complete multipole basis, it can be represented by equivalent operators [36]. Noted that the Wigner-9j symbol in Equation 18 becomes zero when $s=1$ and $k=l$, and therefore $\beta_l^{(1,l)} = 0$. This means that the sum rule of dipole transition can capture the information for electric and magnetic multipoles, $\boldsymbol{Q}$ and $\boldsymbol{M}$ on a complete magnetic multipole basis, and cannot directly apply to electric and magnetic toroidal moments, $\boldsymbol{G}$ and $\boldsymbol{T}$.

Using the relations $\alpha_+^{(1)} + \alpha_-^{(1)} = 0$, the sum over $S_{lm}^{j\pm}$ on the two core states $j_{\pm} = l_c \pm \frac{1}{2}$ is expressed as,

$$S_{lm}^{j+} + S_{lm}^{j-} = [l_c] \beta_l^{(0,l)} \langle \underline{X}_{lm}^{(0,0)} \rangle, \quad (21)$$

suggesting that it gives expectation values for the spinless multipoles. Hereafter, it will be referred to as the spinless sum rule. Similarly, by using a relation $\alpha_+^{(0)} - \frac{l_c+1}{l_c} \alpha_-^{(0)} = 0$, another sum rule can be derived,

$$S_{lm}^{j+} - \frac{l_c+1}{l_c} S_{lm}^{j-} = [l_c] \sqrt{\frac{3(l_c+1)}{l_c}} \left\{ \beta_l^{(1,l-1)} \langle \underline{X}_{lm}^{(1,-1)} \rangle - \beta_l^{(1,l+1)} \langle \underline{X}_{lm}^{(1,1)} \rangle \right\}, \quad (22)$$

which allows for the detection of only spinful multipoles. Hereafter, it will be referred to as the spinful sum rule. In other words, depending on the method of calculating the absorption sum with the core as the

reference, it is possible to extract either spinless or spinful magnetic multipoles selectively.

4. Explicit expression of magnetic multipoles in sum rules

In the present paper, we will examine the relationship between the XAS, XMCD, and XMLD sum rules, and magnetic multipoles concretely using the case of the dipole transition $l_c = 1$ ($2p$ orbitals) $\rightarrow$ $l_v = 2$ ($3d$ orbitals) as an example. The relation between the polarization sum rules and the complete magnetic multipole basis and physical quantity is classified in Table 3.

4.1. Monopole sum rule

The sum rule on the isotropic XAS ($I^{j\pm}_{XAS} = I^{j\pm}_{z} + I^{j\pm}_{+} + I^{j\pm}_{-}$) gives the complete multipole basis of charge monopole $l = 0, m = 0$. Since the spinless monopole is given by $\underline{Q}^{(0,0)}_{00} = \underline{Q}^{(\mathrm{orb})}_{00} = O_{00}$, the spinless sum rule ($s = 0$) is expressed as

$$I^{j+}_{XAS} + I^{j-}_{XAS} = \langle n_h \rangle C, \tag{23}$$

where n_h indicates the number of holes in the l_v state and C is the normalized constant factor including the radial matrix element of the dipole transition and multipoles. On the other hand, the spinful monopole is given by

$$Q^{(1,1)}_{00} = -\sum_{n} C^{00}_{1,-n;1,n} M^{(\mathrm{orb})}_{1,-n} \sigma_{1n} = \frac{1}{\sqrt{3}} \left(\hat{l} \cdot \hat{s} \right), \tag{24}$$

which involves the spin-orbit coupling ($\left(\lambda \hat{l}.\hat{s}\right)$) in the l_v state. Consequently, the intensity of the spinful monopole sum rule is proportional to $Q^{(1,1)}_{00}$, and is expressed as

$$I^{j+}_{XAS} - 2I^{j-}_{XAS} = \langle \hat{l} \cdot \hat{s} \rangle C, \tag{25}$$

where C is the same normalized factor as in Equation 23. This means that when the spin – orbit interaction in l_v is zero, the intensity ratio of I^{j+}_{XAS} to I^{j-}_{XAS} is 2:1, and conversely, as the interaction becomes stronger, the absorption intensity of I^{j-}_{XAS} decreases.

These results suggest that spinful electric dipole transitions offer a pathway to probe the spin-orbit interaction in the valence states. However, in early $3d$ transition metals, such as V and Cr, the L_3/L_2 branching ratio significantly deviates from the expected 2:1 value, tending toward 1:1 due to strong electron-core-hole interaction and the small spin-orbit splitting of the $2p$ core levels [37,38]. This highlights the need for caution when interpreting branching ratios in such systems.

4.2. Dipole sum rule

The sum rule for $l = 1$ represents that for the XMCD spectrum ($I^{j\pm}_{XMCD} = I^{j\pm}_{+} - I^{j\pm}_{-}$) and involves the first-order multipoles associated with the magnetic dipole moment. Here, we consider $m = 0$, that is, $S^{j\pm}_{10} = -\frac{1}{\sqrt{2}}(I^{j\pm}_{+} - I^{j\pm}_{-})$, which gives the component of each dipole moment projected onto the z direction [see Figure 1(a)]. Since the spinless dipole moment is given by $\underline{M}^{(0,0)}_{10} = \underline{M}^{(\mathrm{orb})}_{10} = \underline{l}_z$, the spinless sum rule ($s = 0$) is expressed as

$$I^{j+}_{XMCD} + I^{j-}_{XMCD} = -\frac{1}{2} \langle \underline{l}_z \rangle C, \tag{26}$$

indicating that the sum rule of the XMCD selectively extracts information on orbital angular momentum in magnetization [6].

On the other hand, spinful dipole moments have two components: one is the pure spin represented by $\underline{M}^{(1,-1)}_{10} = C^{10}_{00;10} \underline{Q}^{(\mathrm{orb})}_{00} \underline{\sigma}_z = \underline{\sigma}_z$, and the other is a term arising from the coupling between the electric quadrupole and the spin,

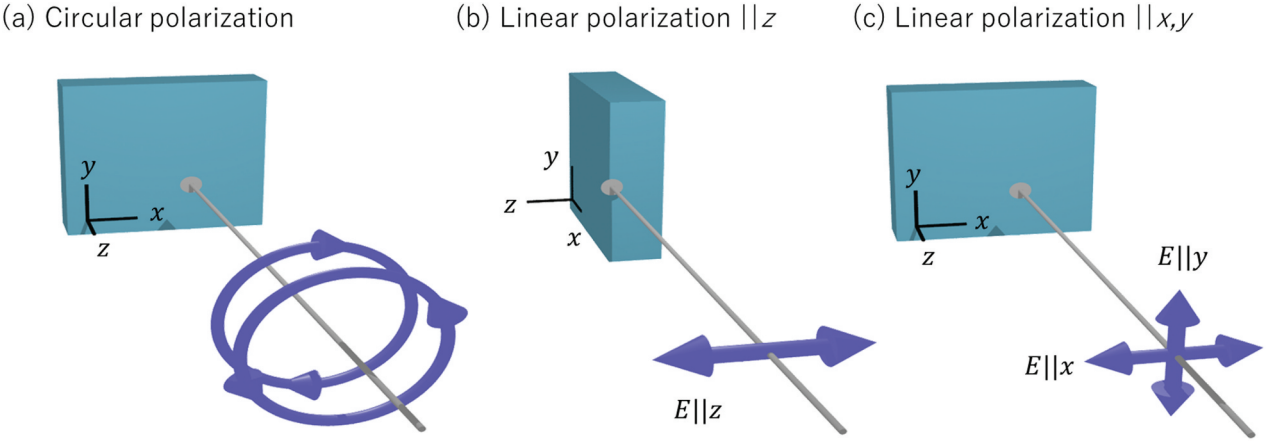

Figure 1. Experimental setup of x-ray absorption with the incident polarization of (a) circular, (b) linear ($E||z$), and (c) linear ($E||x$ and $E||y$).

$$[M_{10}^{(1,1)}]_z = -\sum_n C^{10}_{2,-n;1n} Q^{(\mathrm{orb})}_{2,-n}\sigma_{1n} = \frac{1}{\sqrt{10}}\sum_i (3zr_i - \mathbf{r}^2\delta_{zr_i})\sigma_z \quad (27)$$

with $\boldsymbol{r}$ being operators for the unit vector of position [35]. The latter is proportional to the anisotropic magnetic dipole t_z term [39], which provides information on the anisotropy of the electron spin-density distribution. Consequently, the spinful sum rule ($s = 1$) is expressed as

$$I^{j+}_{\mathrm{XMCD}} - 2I^{j-}_{\mathrm{XMCD}} = -\left(\frac{2}{3}\langle \underline{s}_z\rangle + \frac{7}{3}\langle \underline{t}_z\rangle\right)C, \quad (28)$$

with $t_z = \frac{1}{4}\left(3[l_z(\boldsymbol{l}\cdot\boldsymbol{s})]_+ - 2l^2 s_z\right)$ in the equivalent l orperator form [40].

XMCD is used to separate spin and orbital contributions, and is particularly valuable in ferrimagnetic materials because it allows element-specific evaluation [41]. Additionally, the spinful multipole term t_z has been used to uncover the role of hidden multipoles in magnetic materials. For example, in an exchange-bias Fe/MgO system, an electric-field – driven XMCD response has been observed, which originates from changes in the anisotropic spatial distribution of spin involved with the anisotropic magnetic dipole term t_z [12]. The t_z component of the spinful dipole is a good descriptor for the characteristics of the exchange bias effect and its response to an electric field. Additionally, the t_z term has recently been identified as a key origin of XMCD signals in antiferromagnets lacking net magnetization, as exemplified by chiral antiferromagnetic Mn_3Sn [29,30] and collinear antiferromagnetic (altermagnetic) systems, such as RuO_2 [42] and MnTe [43]. Magnetic materials that exhibit XMCD despite being antiferromagnetic can be classified, within a magnetic multipole basis, as spinful magnetic dipoles; adopting this framework is essential both for categorizing such materials and for interpreting their behavior. Indeed, it has even been theoretically proposed that the spinful magnetic dipole t_z underlies the emergence of anomalous Hall effect in antiferromagnet [44].

4.3. Quadrupole sum rule for out-of-plane XMLD (zXMLD)

The sum rule for $l = 2$ represents that for the XMLD spectrum and involves the second-order multipoles associated with the electronic quadrupole moment. First, we consider $m = 0$, that is, $S^{j\pm}_{20} = \frac{1}{\sqrt{10}}(I^{j\pm}_{+} + I^{j\pm}_{-} - 2I^{j\pm}_{z})$, which shows the difference in x-ray absorption intensity when the polarization is applied within the xy plane and along the out-of-plane direction [see Figure 1(b,c)]. The spinless multipole of the quadrupole moment is given by $\underline{Q}^{(0,0)}_{20} = \underline{Q}^{(\mathrm{orb})}_{20}$, which represents the electronic quadrupole moment $O_{20} = \frac{1}{2}(3z^2 - r^2)$, corresponding to $d_{3z^2-r^2}$ orbital. Therefore, the spinless sum rule ($s = 0$) is expressed as,

$$I^{j+}_{\mathrm{zXMLD}} + I^{j-}_{\mathrm{zXMLD}} = \langle \underline{Q}_{zz}\rangle C, \quad (29)$$

with the equivalent operator $Q_{zz} = \frac{1}{2}(l_z^2 - \frac{1}{3}l^2)$ [36]. This result reflects the anisotropy of charge distribution between the out-of-plane and the in-plane direction.

The spinful electronic quadrupole moments are composed of magnetic dipole and octupole terms. The magnetic dipole one is given by

$$Q^{(1,-1)}_{20} = \sum_n C^{2,0}_{1,-n;1n} M^{(\mathrm{orb})}_{1,-n}\sigma_{1n} = \frac{1}{\sqrt{6}}(3l_z s_z - \boldsymbol{l}\cdot\boldsymbol{s}), \quad (30)$$

indicating the anisotropy of the spin-orbit coupling ($\lambda\boldsymbol{l}\cdot\boldsymbol{s}$), which enables the probing of the magnetocrystalline anisotropy [45]. The equivalent operator is given by $P_{zz} = \frac{1}{2}(3l_z s_z - \boldsymbol{l}\cdot\boldsymbol{s})$ [36,40]. The octupole term in the spinful quadrupole moment is expressed as

$$Q^{(1,1)}_{20} = -\sum_n C^{2,0}_{3,-n;1n} M^{(\mathrm{orb})}_{3,-n}\sigma_{1n} \quad (31)$$

where the magnetic octupole operators are shown in the Table 2. For example, when the spin is oriented along the z-axis, the explicit expression by extracting only the term proportional to s_z is given by

$$M^{(\mathrm{orb})}_{30}\sigma_z = -\frac{3}{2}[zxl_x + zyl_y]_+ s_z + \frac{3}{2}(3z^2 - r^2)l_z s_z \quad (32)$$

which reflects a quantity combining the electric quadrupole and spin-orbit coupling. Consequently, the spinful sum rule is expressed as,

$$I^{j+}_{\mathrm{zXMLD}} - 2I^{j-}_{\mathrm{zXMLD}} = \left(\frac{2}{5}\langle \underline{P_{zz}}\rangle + \frac{3}{5}\langle \underline{R_{zz}}\rangle\right)C, \quad (33)$$

where $R_{zz} = \frac{1}{3}[5l_z(\boldsymbol{l}\cdot\boldsymbol{s})l_z - (l^2 - 2)\boldsymbol{l}\cdot\boldsymbol{s} - (2l^2 + 1)l_z s_z]$ is the equivalent operator of $Q^{(1,1)}_{20}$ [36,40]. In the case of the electric quadrupole sum rule, it is difficult to separately measure the spinful magnetic dipole and magnetic octupole. As a result, it is also useful to express as $I^{j+}_{\mathrm{zXMLD}} - 2I^{j-}_{\mathrm{zXMLD}} = \langle \underline{U}_{zz}\rangle C$ using the total operator $U_{zz} = l_z(\boldsymbol{l}\cdot\boldsymbol{s})l_z - 2l_z s_z - \boldsymbol{l}\cdot\boldsymbol{s}$.

Out-of-plane XMLD has been used to determine magnetic anisotropy, for example in perpendicularly magnetized Fe/MgO films [46] and $Mn_{3-\delta}Ga$ alloys [47]. Since it can detect magnetic multipoles corresponding to the anisotropic components of the spin – orbit interaction [45], it holds promise for estimating the perpendicular magnetic anisotropy energy based on the spinful electronic quadrupole multipoles. Moreover, when a magnetic field is applied to

a magnetic octupole state, the response corresponds to R_{zz} multipole, suggesting potential applicability for detection and quantitative evaluation of magnetic octupole order through the XMLD sum rule such as in CeB_6 [48].

4.4. Quadrupole sum rule for in-plane XMLD (xyXMLD)

Next, we consider $l=2$ and $m=\pm2$ cases, $S^{j\pm}_{2,\pm2}=\frac{3}{\sqrt{15}}P^{j\pm}_{\pm1,\mp1}$, corresponding to the cross term of left and right circular polarization, which is not possible to directly observe in absorption which can only describe the polarization of the incident x-rays as shown in Equation 8. Therefore, we consider the combination of sum rules for $m=\pm2$, and then it becomes clear that the signal can be observed as an in-plane xyXMLD $[I^{j\pm}_{\mathrm{xyXMLD}}=I^{j\pm}_{x}-I^{j\pm}_{y}]$ component using $S^{j\pm}_{2,2}+S^{j\pm}_{2,-2}=\frac{3}{\sqrt{15}}(I^{j\pm}_{x}-I^{j\pm}_{y})$ [see Figure 1(c)]. The corresponding spinless multipole of quadrupole moment is given by $\underline{Q}^{(\mathrm{orb})}_{2,2}+\underline{Q}^{(\mathrm{orb})}_{2,-2}$; consequently, the spinless sum rule is expressed as

$$I^{j+}_{\mathrm{xyXMLD}}+I^{j-}_{\mathrm{xyXMLD}}=\langle\underline{Q}_{x^2-y^2}\rangle C, \tag{34}$$

with the operator equivalent $Q_{x^2-y^2}\equiv(l_y^2-l_x^2)/6$, reflecting the anisotropic charge distribution within the xy-plane.

The spinful electronic quadrupole moments are composed of magnetic dipole and octupole terms. The magnetic dipole one is given by

$$Q^{(1,-1)}_{x^2-y^2}\equiv Q^{(1,-1)}_{2,2}+Q^{(1,-1)}_{2,-2}=\frac{1}{2}(l_xs_x-l_ys_y) \tag{35}$$

with $Q^{(1,-1)}_{2,\pm2}=\sum_n C^{2,\pm2}_{1,\pm2-n;1n}M^{(\mathrm{orb})}_{1,\pm2-n}\sigma_{1n}$, indicating the anisotropy of the spin-orbit coupling within the xy-plane. On the other hand, the octupole term is expressed as

$$Q^{(1,1)}_{2,\pm2}=-\sum_n C^{2,\pm2}_{3,\pm2-n;1n}M^{(\mathrm{orb})}_{3,\pm2-n}\sigma_{1n} \tag{36}$$

where the magnetic octupole operators are given in Table 2. For example, when the spin is oriented along the z-axis, extracting only the term proportional to s_z results in

$$(M^{(\mathrm{orb})}_{3,2}+M^{(\mathrm{orb})}_{3,-2})\sigma_z=\sqrt{\frac{15}{2}}[xzl_x-yzl_y]_+s_z+(x^2-y^2)l_zs_z, \tag{37}$$

which reflects a quantity combining the electric quadrupole and spin-orbit coupling involving the in-plane anisotropy. Consequently, the spinful sum rule for xyXMLD is expressed as

$$I^{j+}_{\mathrm{xyXMLD}}-2I^{j-}_{\mathrm{xyXMLD}}=\left(\frac{2}{5}\langle\underline{P}_{x^2-y^2}\rangle+\frac{3}{5}\langle\underline{R}_{x^2-y^2}\rangle\right)C, \tag{38}$$

with the operator equivalents $P_{x^2-y^2}\equiv\frac{2}{3}(l_xs_x-l_ys_y)$ and $R_{x^2-y^2}\equiv\frac{2}{9}\{l_y(\boldsymbol{l}\cdot\boldsymbol{s})l_y-l_x(\boldsymbol{l}\cdot\boldsymbol{s})l_x\}$. These operators reflect the in-plane anisotropy of the spin – orbit interaction.

For example, such in-plane XMLD has been employed to visualize the spatial domain structure of the Néel vector in antiferromagnetic NiO [49]. With the present formalism, it is expected that information on anisotropic spin – orbit interactions can be extracted from the integrated XMLD spectrum, providing crucial insight for evaluating the magnetic anisotropy energy of antiferromagnetic materials. Additionally, since these electric quadrupole moments have the same symmetry as the magnetic toroidal quadrupole moment with the applied magnetic field, it is expected to detect the anisotropy of the electronic states in d-wave altermagnets such as in MnF_2 [50] and $NiCo_2O_4$ [51].

5. Conclusion

In this study, we have reconsidered the sum rules for X-ray absorption spectroscopy based on a complete magnetic multipole basis. We have demonstrated that it naturally derives the anisotropic magnetic dipole term in the XMCD, which plays important role in the s-wave altermagnetic system. Additionally, we have shown that the sum rules for out-of-plane and in-plane X-ray Magnetic Linear Dichroism (XMLD) can be derived using the electric quadrupole contributions. This approach provides a unified theoretical framework to analyze and interpret dichroic signals in a wide range of magnetic materials. Our findings not only enhance the understanding of XMCD and XMLD but also pave the way for further research in complex magnetic structures. Future studies incorporating this multipole-based methodology could further refine our insights into spin-orbit interactions and hidden magnetic orderings in advanced magnetic materials.

Notes

1. Here, we use the following relation.

$$\sum\nolimits_{m_j}C^{jm_j}_{l_cm_c;\frac{1}{2}m_s}C^{jm_j}_{l_cm_c';\frac{1}{2}m_s'}=\frac{j_\pm+\frac{1}{2}}{2l_c+1}C^{\frac{1}{2}m_s}_{\frac{1}{2}m_s';00}C^{l_cm_c}_{l_cm_c';00}$$

$$\pm\sum\nolimits_{n=-1}^{1}\frac{\sqrt{3l_c(l_c+1)}}{2l_c+1}C^{\frac{1}{2}m_s}_{\frac{1}{2}m_s';1n}C^{l_cm_c}_{l_cm_c';1,-n},$$

2. The function for finite summation involving four Clebsh-Gordan coefficients used here is found in https://functions.wolfram.com/07.38.23.0029.01.

Acknowledgments

The authors thank T. Arima and M. Mizumaki for the productive discussion. This project is partly supported by the Japan Society for the Promotion of Science (JSPS) KAKENHI (19H04399, 24K03205, and 24H01685). This work was supported by MEXT Quantum Leap Flagship Program (MEXT Q-LEAP) Grant Number JPMXS0118068681. This work is also partially supported by CREST(JPMJCR1861 and JPMJCR2435), Japan Science and Technology Agency (JST).

Disclosure statement

No potential conflict of interest was reported by the author(s).

Funding

This work was supported by the Core Research for Evolutional Science and Technology [JPMJCR1861, JPMJCR2435]; Japan Society for the Promotion of Science [JP19H04399, JP23K17145, JP24K03205, JP24H01685, JP25K0338]; Ministry of Education, Culture, Sports, Science and Technology [JPMXS0118068681]; PRESTO [JPMJPR2102].

ORCID

Y. Yamasaki http://orcid.org/0000-0002-8560-3462

References

[1] de Groot FMF, Kotani A. Core level spectroscopy of solids. Cambridge (UK): Cambridge University Press; 2008.
[2] Schütz G, Wagner W, Wilhelm W, et al. Absorption of circularly polarized x rays in iron. Phys Rev Lett. 1987;58(7):737. doi: 10.1103/PhysRevLett.58.737
[3] Stöhr J. Exploring the microscopic origin of magnetic anisotropies with X-ray magnetic circular dichroism (XMCD) spectroscopy. J Magn Magn Mater. 1999;200(1–3):470. doi: 10.1016/S0304-8853(99)00407-2
[4] Alders D, Tjeng LH, Voogt FC, et al. Temperature and thickness dependence of magnetic moments in NiO epitaxial films. Phys Rev B. 1998;57(18):11623. doi: 10.1103/PhysRevB.57.11623
[5] van der Laan G, Figueroa AI. X-ray magnetic circular dichroism—a versatile tool to study magnetism. Coord Chem Rev. 2014;277–278:95. doi: 10.1016/j.ccr.2014.03.018
[6] Thole BT, Carra P, Sette F, et al. X-ray circular dichroism as a probe of orbital magnetization. Phys Rev Lett. 1992;68(12):1943. doi: 10.1103/PhysRevLett.68.1943
[7] Carra P, Thole BT, Altarelli M, et al. X-ray circular dichroism and local magnetic fields. Phys Rev Lett. 1993;70(5):694. doi: 10.1103/PhysRevLett.70.694
[8] Chen CT, Idzerda YU, Lin H-J, et al. Experimental confirmation of the X-Ray magnetic circular dichroism sum rules for iron and cobalt. Phys Rev Lett. 1995;75(1):152. doi: 10.1103/PhysRevLett.75.152
[9] Teramura Y, Tanaka A, Jo T. Effect of coulomb interaction on the X-Ray magnetic circular dichroism spin sum rule in 3 d transition elements. J Phys Soc Jpn. 1996;65(4):1053. doi: 10.1143/JPSJ.65.1053
[10] Bi C, Liu Y, Newhouse-Illige T, et al. Reversible control of co magnetism by voltage-induced oxidation. Phys Rev Lett. 2014;113(26):267202. doi: 10.1103/PhysRevLett.113.267202
[11] Zhang B, Sun C-J, Lü W, et al. Electric-field-induced strain effects on the magnetization of a P $r_{0.67}$ S $r_{0.33}$ Mn O_3 film. Phys Rev B. 2015;91(17):174431. doi: 10.1103/PhysRevB.91.174431
[12] Miwa S, Matsuda K, Tanaka K, et al. Voltage-controlled magnetic anisotropy in Fe|MgO tunnel junctions studied by x-ray absorption spectroscopy. Appl Phys Lett. 2015;107(16):162402. doi: 10.1063/1.4934568
[13] Chang S-J, Chung M-H, Kao M-Y, et al. $GdFe_{0.8}$ $Ni_{0.2}$ O_3: a multiferroic material for low-power spintronic devices with high storage capacity. ACS Appl Mater Interfaces. 2019;11(34):31562. doi: 10.1021/acsami.9b11767
[14] Ishii Y, Yamasaki Y, Kozuka Y, et al. Microscopic evaluation of spin and orbital moment in ferromagnetic resonance. Sci Rep. 2024;14(1):15504. doi: 10.1038/s41598-024-66139-1
[15] Chen CT, Sette F, Ma Y, et al. Symmetry-breaking instabilities of spatial parametric solitons. Phys Rev B. 1997;56(5):R4959. doi: 10.1103/PhysRevE.56.R4959
[16] Scholl A, Stohr J, Luning J, et al. Observation of antiferromagnetic domains in epitaxial thin films. Science. 2000;287(5455):1014. doi: 10.1126/science.287.5455.1014
[17] Nakatsuji S, Kiyohara N, Higo T. Large anomalous hall effect in a non-collinear antiferromagnet at room temperature. Nature. 2015;527(7577):212. doi: 10.1038/nature15723
[18] Higo T, Man H, Gopman DB, et al. Large magneto-optical Kerr effect and imaging of magnetic octupole domains in an antiferromagnetic metal. Nat Photonics. 2018;12(2):73. doi: 10.1038/s41566-017-0086-z
[19] Solovyev IV. Magneto-optical effect in the weak ferromagnets $LaMO_3$ (M= Cr, Mn, and Fe). Phys Rev B. 1997;55(13):8060. doi: 10.1103/PhysRevB.55.8060
[20] Noda Y, Ohno K, Nakamura S. Momentum-dependent band spin splitting in semiconducting MnO_2: a density functional calculation. Phys Chem Chem Phys. 2016;18(19):13294. doi: 10.1039/C5CP07806G
[21] Okugawa T, Ohno K, Noda Y, et al. Weakly spin-dependent band structures of antiferromagnetic perovskite $LaMO_3$ (M = cr, Mn, Fe). J Phys Condens Matter. 2018;30(7):075502. doi: 10.1088/1361-648X/aa9e70
[22] Naka M, Hayami S, Kusunose H, et al. Spin current generation in organic antiferromagnets. Nat Commun. 2019;10(1). doi: 10.1038/s41467-019-12229-y
[23] Ahn K-H, Hariki A, Lee K-W, et al. Antiferromagnetism in RuO_2 as d -wave pomeranchuk instability. Phys Rev B. 2019;99(18):184432. doi: 10.1103/PhysRevB.99.184432
[24] Šmejkal L, Gonzalez-Hernandez R, Jungwirth T, et al. Crystal time-reversal symmetry breaking and spontaneous hall effect in collinear antiferromagnets. Sci Adv. 2020;6(23):eaba9399. doi: 10.1126/sciadv.aaz8809

[25] Šmejkal L, Gonzalez-Hernandez R, Jungwirth T, et al. Emerging research landscape of altermagnetism. Science. 2022;375:70.
[26] Šmejkal L, Jungwirth T, Sinova J. Altermagnetism: a new class of magnetism with spin-split electronic states protected by symmetry. Nat Rev Mater. 2023;8:653.
[27] Hariki A, Dal Din A, Amin OJ, et al. X-Ray magnetic circular dichroism in altermagnetic α -MnTe. Phys Rev Lett. 2024;132(17):176701. doi: 10.1103/PhysRevLett.132.176701
[28] Amin OJ, Din AD, Golias E, et al. Nanoscale imaging and control of altermagnetism in MnTe. Nature. 2024;636(8042):348. doi: 10.1038/s41586-024-08234-x
[29] Yamasaki Y, Nakao H, Arima T-H. Augmented magnetic octupole in Kagomé 120-degree antiferromagnets detectable via X-ray magnetic circular dichroism. J Phys Soc Jpn. 2020;89(8):083703. doi: 10.7566/JPSJ.89.083703
[30] Sasabe N, Kimata M, Nakamura T. Presence of X-Ray magnetic circular dichroism signal for zero-magnetization antiferromagnetic state. Phys Rev Lett. 2021;126(15):157402. doi: 10.1103/PhysRevLett.126.157402
[31] Kimata M, Sasabe N, Kurita K, et al. X-ray study of ferroic octupole order producing anomalous hall effect. Nat Commu. 2021;12(1):5582. doi: 10.1038/s41467-021-25834-7
[32] Sakamoto S, Higo T, Shiga M, et al. Observation of spontaneous x-ray magnetic circular dichroism in a chiral antiferromagnet. Phys Rev B. 2021;104(13):134431. doi: 10.1103/PhysRevB.104.134431
[33] Sakamoto S, Higo T, Kotani Y, et al. Bulk and surface uniformity of magnetic and electronic structures in epitaxial W / Mn_3 Sn / MgO films revealed by fluorescence- and electron-yield x-ray magnetic circular dichroism. Phys Rev B. 2024;110(6):L060412. doi: 10.1103/PhysRevB.110.L060412
[34] Kusunose H, Oiwa R, Hayami S. Complete multipole basis set for single-centered electron systems. J Phys Soc Jpn. 2020;89(10):104704. doi: 10.7566/JPSJ.89.104704
[35] Hayami S, Kusunose H. Unified Description of electronic orderings and cross correlations by complete multipole representation. J Phys Soc Jpn. 2024;93(7):072001. doi: 10.7566/JPSJ.93.072001
[36] Carra P, König H, Thole B, et al. Magnetic X-ray dichroism. Physica B Condens Matter. 1993;192(1–2):182. doi: 10.1016/0921-4526(93)90119-Q
[37] Ankudinov AL, Nesvizhskii AI, Rehr JJ. Dynamic screening effects in x-ray absorption spectra. Phys Rev B Condens Matter. 2003;67(11):115120. doi: 10.1103/PhysRevB.67.115120
[38] Schwitalla J, Ebert H. Electron core-hole interaction in the X-Ray absorption spectroscopy of 3 d transition metals. Phys Rev Lett. 1998;80(20):4586. doi: 10.1103/PhysRevLett.80.4586
[39] Oguchi T, Shishidou T. Anisotropic property of magnetic dipole in bulk, surface, and overlayer systems. Phys Rev B. 2004;70(2):024412. doi: 10.1103/PhysRevB.70.024412
[40] van der Laan G. Angular momentum sum rules for x-ray absorption. Phys Rev B. 1998;57(1):112. doi: 10.1103/PhysRevB.57.112
[41] Bitla Y, Chin Y-Y, Lin J-C, et al. Origin of metallic behavior in $NiCo_2O_4$ ferrimagnet. Sci Rep. 2015;5(1):15201. doi: 10.1038/srep15201
[42] Sasabe N, Mizumaki M, Uozumi T, et al. Ferroic order for anisotropic magnetic dipole term in collinear antiferromagnets of (t_2 g)4 system. Phys Rev Lett. 2023;131(21):216501. doi: 10.1103/PhysRevLett.131.216501
[43] Amin O, Dal Din A, Golias E, et al. Nanoscale imaging and control of altermagnetism in MnTe. Nature. 2024;636(8042):348. doi: 10.1038/s41586-024-08234-x
[44] Hayami S, Kusunose H. Essential role of the anisotropic magnetic dipole in the anomalous hall effect. Phys Rev B. 2021;103(18):L180407. doi: 10.1103/PhysRevB.103.L180407
[45] van der Laan G. Magnetic linear X-Ray dichroism as a probe of the magnetocrystalline anisotropy. Phys Rev Lett. 1999;82(3):640. doi: 10.1103/PhysRevLett.82.640
[46] Okabayashi J, Koo JW, Sukegawa H, et al. Perpendicular magnetic anisotropy at the interface between ultrathin Fe film and MgO studied by angular-dependent x-ray magnetic circular dichroism. Appl Phys Lett. 2014;105(12):122408. doi: 10.1063/1.4896290
[47] Okabayashi J, Miura Y, Kota Y, et al. Detecting quadrupole: a hidden source of magnetic anisotropy for manganese alloys. Sci Rep. 2020;10(1):9744. doi: 10.1038/s41598-020-66432-9
[48] Matsumura T, Yonemura T, Kunimori K, et al. Magnetic field induced 4 f octupole in CeB_6 probed by resonant X-Ray diffraction. Phys Rev Lett. 2009;103(1):017203. doi: 10.1103/PhysRevLett.103.017203
[49] Kinoshita T, Arai K, Fukumoto K, et al. Magnetic linear dichroism of antiferromagnetic domains in NiO observed by X-ray absorption spectroscopy. J Phys Soc Jpn. 2012:81(7):073702. doi:10.1143/JPSJ.81.073702
[50] Higuchi T, Kuwata-Gonokami M. Control of antiferromagnetic domain distribution via polarization-dependent optical annealing. Nat Commun. 2016;7(1):10720. doi: 10.1038/ncomms10720
[51] Koizumi H, Yamasaki Y, Yanagihara H. Quadrupole anomalous hall effect in magnetically induced electron nematic state. Nat Commun. 2023;14(1):8074. doi: 10.1038/s41467-023-43543-1